Journal of Power Sources 196 (2011) 3414–3419

Contents lists available at ScienceDirect

Journal of Power Sources

journal homepage: www.elsevier.com/locate/jpowsour

Effect of discharge rate on charging a lead-acid battery simulated by mathematical model

Mikael Cugnet, Bor Yann Liaw*

Hawaii Natural Energy Institute, SOEST, University of Hawaii at Manoa, 1680 East-West Road, POST 109, Honolulu, HI 96822, USA

ARTICLE INFO

Article history:
Received 27 March 2010
Received in revised form 17 June 2010
Accepted 28 July 2010
Available online 6 August 2010

Keywords:
Valve-regulated lead-acid (VRLA) battery
Mathematical models
Charging efficiency

ABSTRACT

To simulate lead-acid battery (LAB) charging has never been an easy task due to the influences of: (1) secondary reactions that involve gas evolution and recombination and grid corrosion, (2) prior end-of-discharge (EOD) and rest conditions; and (3) complexity caused by charging algorithm. In this work, successful results have been obtained with considerations of internal oxygen cycle and gas phase in the valve-regulated lead-acid (VRLA) cells. The success is first attributed to the satisfactory validation of a mathematical model that has been able to simulate discharge regimes with various rates consistently. The model has been subsequently used to simulate a galvanostatic charge regime performed at *C*/10. The results give a better understanding of the role each electrode played in the polarization, the nature of the polarization (constituted by reaction kinetics and mass transport), and the charging efficiency. We were able to extrapolate the simulation results to rates beyond what the model has been validated for, and the results are still consistent, confirming some experimental observations, notably the maximum charging rate specified by most LAB manufacturers.

1. Introduction

Mathematical model and simulation remain under-utilized by the battery industry, not only because of the complexity involved in the model development, but also due to the lack of accurate prediction for practical application. Accurate battery model and simulation provides insightful information beyond what laboratory testing can, and such knowledge can be applied to an extended range of operating conditions that may not be feasible from laboratory testing. Therefore, the potential presented by modeling and simulation is attractive, especially at times when interests on battery engineering, energy storage, power management, and hybridization of power sources are growing.

Many mathematical models on lead-acid batteries (LAB) have been published in the literature [1–17] for simulation from a single electrode to a complete pack. The modeling capabilities have been improved almost as fast as the computing power that enables them. To date, many programming languages and platforms are available for developing battery model on a personal computer from scratch. The value of using model simulation to improve battery value chain remains to be validated by the industry. One of the vital issues is the accuracy and degree of fidelity a model can deliver, with an implication of how confident one can vest on such predictions.

As exemplified among the work in the citations, most of the LAB mathematical models have focused on battery discharge behavior; thus, only eight among the 17 in the citations presented validation in charge regime [6,9–13,15,17]. However, none of these references, or any other in the literature as far as we know, has shown simulation of charge regimes in a valve-regulated lead-acid (VRLA) cell after it undergoes discharge regimes that may differ over a wide range of rates (such as *C*/20 to 10*C*). It is important to note that it is more complicated to simulate the charge regime than the discharge for three reasons. First, secondary reactions including oxygen and hydrogen evolution, oxygen reduction (i.e., gas recombination), and grid corrosion, cannot be neglected in charge, and they affect the battery voltage, charging efficiency, and life expectancy. Secondly, the initial condition in the charge regime is influenced by the end-of-discharge (EOD) and rest conditions. Thirdly, the LAB charge regime is often composed of more than a single step; typically, it comprises constant current (CC) and constant voltage (CV) regimes, with additional CC trickle charging. The complexity requires a model to handle a set of more complicated boundary conditions and parameters that were not encountered in a typical discharge regime.

Recently, we have investigated the Peukert's law beyond the context of empirical observations using a mathematical model [18]. In that work we offered a comprehensive understanding of the Peukert's behavior in LAB, which appeared highly sensitive to local conditions the electrodes experience. We showed that a conventional LAB mathematical model with refinement on only three rate-dependent parameters (accessible active surface area, tortuos-

* Corresponding author. Tel.: +1 808 956 2339; fax: +1 808 956 2336.
E-mail address: bliaw@hawaii.edu (B.Y. Liaw).

0378-7753/$ – see front matter © 2010 Elsevier B.V. All rights reserved.
doi:10.1016/j.jpowsour.2010.07.089

ity exponent, and maximum capacity density of the active material) is able to produce accurate results, without tweaking other empirical parameters in the model. We demonstrated that it is important to consider these rate-dependent parameters with other critical parameters in the model in accordance with experimental data provided by the manufacturer or published in the literature.

In this work, we use the same mathematical model as reported in Refs. [17,18], and incorporate additional equations to address oxygen recombination cycle, to simulate the discharge and charge regimes of a VRLA battery (12 V, 10 Ah) and the fidelity of the simulation is compared with experimental data. We illustrate that charge regimes could be simulated accurately when the battery goes through discharge regimes at various rates. In the first illustration, a charge regime of a simple galvanostatic mode performed at *C*/10 is demonstrated. In the second example, simulations of galvanostatic charges at various rates are presented to show the fidelity of the simulation achieved beyond the validated range of operation. The impacts of charge rate on battery charging efficiency and life expectancy are discussed.

2. Experimental

A battery manufacturer provides the experimental data used in this paper in order to develop a modeling tool that can be used for battery design. The data come from the test of a VRLA battery (12 V, 10 Ah) that has been discharged at 25 °C using various rates of discharge (*C*/20, *C*/5, *C*, 3*C*, 6*C*, and 10*C*). Data related to the rest period (duration unknown), if any, and the temperature excursion in the battery are not available. After each discharge, a galvanostatic charge at *C*/10 was applied to the battery at the same temperature. The charge duration was imposed to recharge 130% of the capacity that was extracted from the prior discharge. The extent of the recharge was designed to collect data in the oxygen recombination regime for model validation.

The battery manufacturer also provided the critical parameters to facilitate the electrochemical LAB model development. These parameters include the geometry of the electrodes, separator, cell, and monoblock, electrical resistance of the grid, porosity of the electrode matrices, headspace in each cell for gas accumulation, initial concentration and volume of the sulfuric acid, exchange current density of the oxygen recombination, acid conductivity, and other relevant information that is needed for the model.

The mathematical model used in this work is modified from the one that was recently published [17,18]. To simulate the charge regime, some additional features are required in the model. Two integration variables need to take into account the gas volume contained in electrodes and separator, and the current density consumed by the oxygen recombination cycle. These two integration variables are then used in four ordinary differential equations defining the partial pressure of oxygen, the number of moles of oxygen, the overall gas volume, and the pressure within the cell (see Eqs. (18)–(21) from Ref. [6]). The battery is treated as a close and isothermal system with uniform pressure.

3. Results and discussion

Through careful analysis of the experimental data and use of a refined model with three rate-dependent parameters [18]; properly taking into considerations the surface area, tortuosity, and maximum capacity, we were able to obtain satisfactory results for the VRLA battery in a wide range of discharge regimes, from *C*/20 to 10*C*, as shown in Fig. 1. We have previously shown [18] that without proper refinement of the three rate-dependent parameters, it is not possible to use the same set of parameters provided by the manufacturer to simulate discharge regimes over a wide range of rates

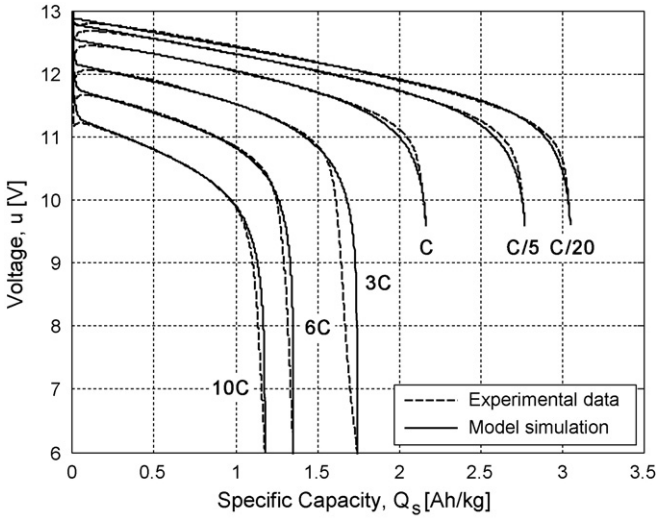

Fig. 1. Comparison of the simulated (solid curve) and experimentally measured (dashed curve) discharge curves at various rates.

accurately. The successful demonstration in Fig. 1 confirms that the refinement with the accessible active area, morphology (tortuosity), and capacity density of the electrodes allows us to simulate VRLA cells over a significant range of rates. This capability may be extended to different battery types, sizes, and even temperatures (unpublished results).

It is important to note that the refinement of these rate-dependent parameters is by no means a trial-and-error process. On the contrary, the three rate-dependent parameters are used to characterize changes related to only one physical phenomenon – a proper account of electrochemically active surface area at the electrode–electrolyte interface which changes with electrode utilization coefficient (EUC) for various discharge rates. The active surface area has been considered dependent of EUC in prior lead-acid cell models [1]. However, it has been considered independent of the discharge rate in all models published so far, which is not in agreement with experimental data obtained by scanning electron microscopy and surface area analysis. In fact, Wales and Simon [19,20] demonstrated that the surface area of the active material increases as discharge current density increases, for both electrodes.

The average error that represents the model accuracy for each rate is 0.6% (74 mV), which is quite acceptable for many applications and close to the results previously obtained with a flooded LAB [17]. At low rates, the simulation results are quite satisfactory. At high rates, more deviation appears; especially near the EOD, which is usually difficult to fit. Considering a battery module is composed of plates in parallel and cells in series that are not exactly identical, it is inevitable that the simulation accuracy will be compromised. The slight variations among the plates and the cells shall cause an internal imbalance, making them reach different depths-of-discharge (DOD) at the EOD. The measured battery voltage at the EOD is the sum of these cells at different DODs, which makes the simulation very challenging without accommodating specific characteristics in each cell. Part of the simulation error also comes from the "coup de fouet" phenomenon (see Ref. [21], p. 288) in the beginning of the discharge regime, which was not taken into account in the model.

Fig. 2 shows the results obtained in the charge regime at *C*/10 with the same VRLA battery when it undergoes discharge regimes (from left to right) at 10*C*, 6*C*, 3*C*, *C*, *C*/5, and *C*/20, respectively. The average error for each charge is 0.6% (84 mV), which is similar to what we received in the discharge regime and considered acceptable for most applications. To yield such accurate simulation

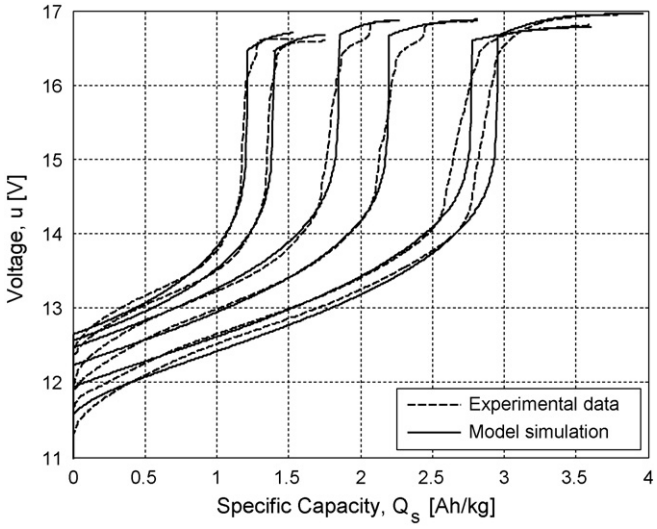

Fig. 2. Comparison of the simulated (solid curve) and experimentally measured (dashed curve) charge curves at $C/10$ obtained after 10C, 6C, 3C, C, $C/5$, and $C/20$ discharge regimes (from left to right).

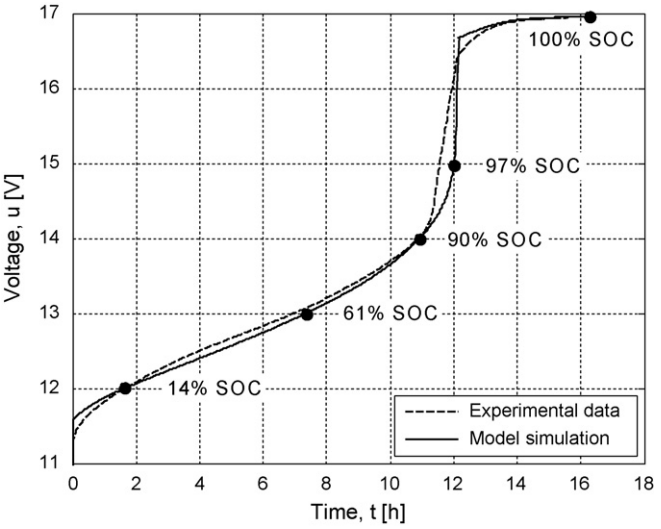

Fig. 3. Comparison of the simulated (solid curve) and experimentally measured (dashed curve) charge curves at $C/10$ obtained after the $C/20$ discharge along with the SOC evolution.

slight adjustments in the three parameters were made. For example, the capacity density of electrode active materials was allowed to fluctuate around 2% of its original value, which is reasonable and within the range experimentally observed. The specific interfacial active area at the fully charged condition was allowed to vary after two high rates (C and 3C) discharge regimes, which could be a consequence of a change in the rest period following these regimes. It should be noted that the rest period has an impact on the electrode active area, as reported by Yamaguchi et al. recently [22]. They showed that chemically formed lead sulfate crystals were different in appearance from the electrochemically formed ones. Another adjustment was made on exchange current density of oxygen recombination, which increases in the charge regime conducted after high rate discharges (e.g., above 3C). Two possible justifications may account for this adjustment. First, the battery may have lost a noticeable amount of water during charging, due to the 130% charge factor applied. According to Berndt [23], considering the worst scenario that there is no oxygen recombination, the water loss (calculated from Eq. (65) in Ref. [17]) could account for this current density increase, since the battery could have lost about 5% of the water contained in the electrolyte. However, it is also known that the maximum rate for the internal oxygen cycle in AGM batteries is about $C/10$ [23], which is difficult to come up with the 5% water loss. A more likely explanation for the parameter adjustment comes from the change in the saturation of the electrolyte in the separator other than excessive water loss. Due to this phenomenon, VRLA batteries may behave like flooded ones in the first few cycles. Further investigations are needed to fully understand the role each secondary reaction plays during the last part of the LAB charge process.

Fig. 3 shows the progression of battery voltage versus time in the $C/10$ charge regime between the experimental data and simulation. The percentage of state-of-charge (SOC) was calculated for a few interesting points on the curve. The figure clearly shows the extent of charge the galvanostatic regime can achieve. The battery was 90% charged when it reached 14 V. Ideally, extrapolating from that result, to charge the battery fully in the galvanostatic mode, current has to be maintained beyond 16.5 V. This condition is however difficult to reach in practical applications, since oxygen recombination cycle and other parasitic reactions may divert the current to prevent a full charge return. It is therefore quite inefficient to charge the battery beyond this point with CC regime, since most current may be used in the secondary reactions.

There is a discontinuity in the simulated curve appeared after 12 h, contrary to the smooth curve from the experiment. This is the result from the simulation of the oxygen evolution at the positive electrode and recombination at the negative, respectively. Such discrepancy between the simulation and experimental results suggests that the charging process is more complex than that comprised of the primary de-sulfation and secondary oxygen recombination cycle at the electrodes. In addressing this issue, for instance, Bernardi et al. [15], in their recent work proposed a dissolution-transport mechanism at the negative electrode. It is also plausible to include a thin proton-conducting surface layer on the positive electrode [24] to buffer surface proton concentration and modify the concentration profile near the electrode–electrolyte interface, so the concentration change would not be so abrupt.

Fig. 4 allows a better representation on the evolution of SOC and charging efficiency during the CC regime at $C/10$. Before 75% SOC, the current is primarily used for the primary reactions. Above 75% SOC, the oxygen evolution occurs at a significant rate and the charging efficiency starts to decrease. At 95% SOC, the charging efficiency

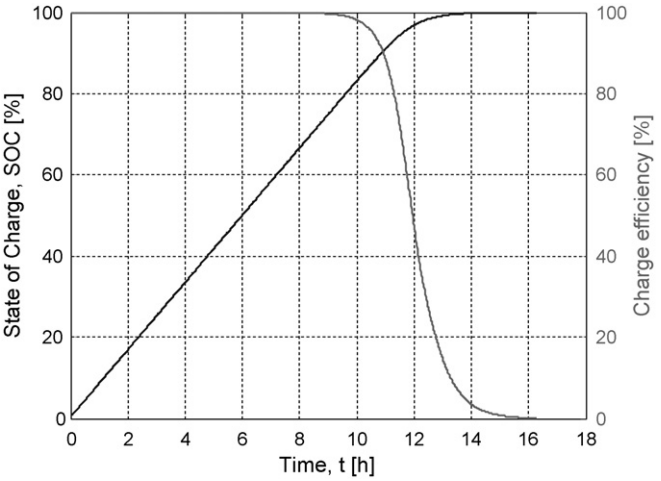

Fig. 4. State-of-charge (black) and charging efficiency (grey) with respect to charge duration.

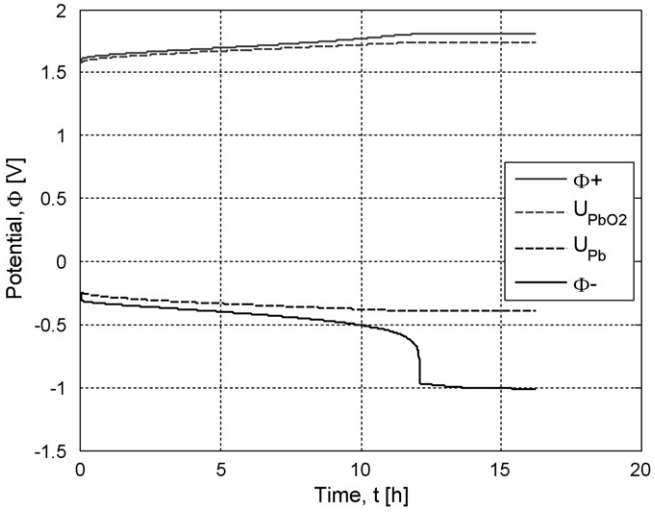

Fig. 5. Electrical potentials (solid curve) and thermodynamic potentials (dashed curve) of the positive and negative electrodes.

is already down to 50%. At the end-of-charge (EOC), the battery received charge equals to 130% of what has been discharged. Such CC charging regime is therefore inefficient and impractical for real use. This underscores the reason manufacturers often suggest the use of CV charge regime near the onset of gas evolution to improve charging efficiency and minimize gas evolution.

The model may determine polarization potential variations on each electrode to reflect the polarization contribution from each reaction, primary or secondary, and the underlying kinetics. Fig. 5 shows the electrochemical (solid curves) and chemical (dashed curves) potentials of each individual electrode calculated for the charge regime. By convention, all potentials refer to the standard hydrogen electrode (SHE). The voltage difference between the two solid curves represents the cell voltage evolution in the charging process. The disparities between the two sets of curves indicate that the surface proton concentration on the electrode and the acid concentration in the liquid near the surface at the two electrodes are growing in magnitude through the charging process, respectively. The potential drop due to ohmic resistance is quite negligible at this low charging rate; therefore, the disparities, depicting the increasing concentration polarization by the reaction kinetics, especially by oxygen evolution and recombination, become evident and comprehensible.

From 0% to 90% SOC, little oxygen was evolved and recombined during this prime charging period. According to Bernardi et al. [15], two major processes dictate the cell behavior during this period: (1) variations of the accessible surface area on the electrodes dictate the first. As $PbSO_4$ transforms to more electronically conductive active materials at the electrode surfaces, increasingly accessible surface area for the electrochemical reaction uncovers. Meanwhile, as the surface area of the $PbSO_4$ particles diminishes during charge, the lead ion concentration is depleting in the charging process, since the dissolution rate of $PbSO_4$ may fall behind the charge rate; and (2) the effect of acid concentration dictates the other process, which affects only the PbO_2 positive electrode potential response. Fig. 5 shows that changes in the PbO_2 electrode potential (solid curve) follow the variations in the thermodynamic potential (dashed curve). The initial sharp rise in potential in the range of 0–5% SOC is due to the change in sulfuric acid concentration. It is important to point out that the experimental results in Fig. 3 also indicate an initial sharp rise in potential and the model predicts a similar initial potential rise attributed to the PbO_2 electrode.

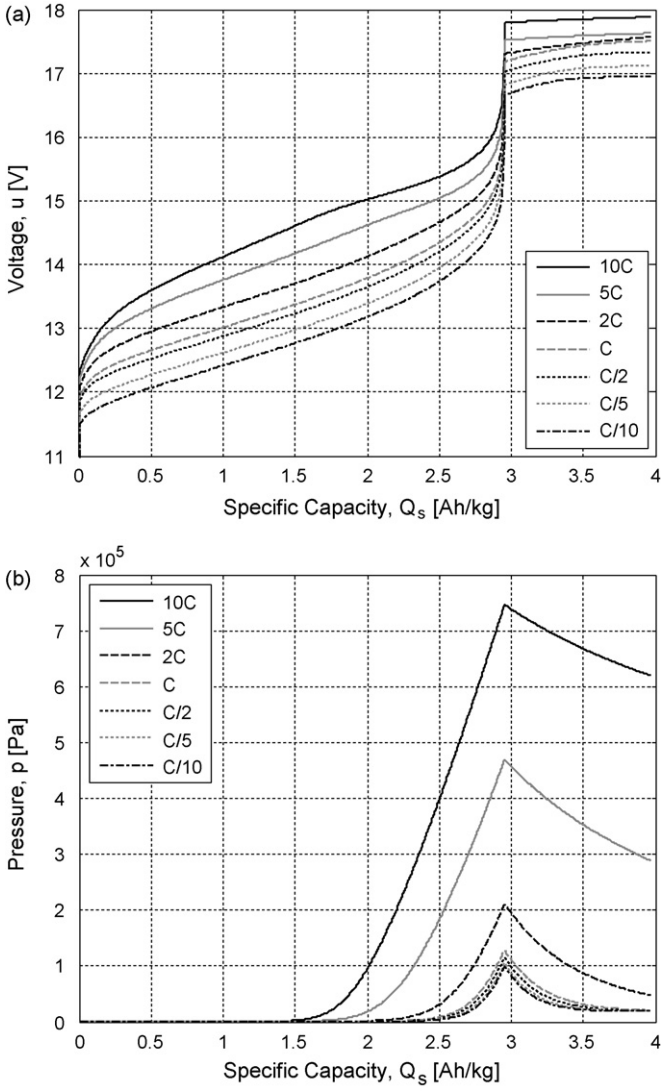

Fig. 6. Simulated (a) voltage and (b) pressure curves at various rates in charge regime.

After the onset of significant oxygen evolution at approximately 90% SOC, the cell voltage variation becomes more complex since it is affected by four reactions as opposed to only two at low SOCs. The simulation results show a rapid potential decrease at the negative electrode due to an increasing fraction of the current diverted to oxygen recombination, while oxygen is being increasingly produced at the positive electrode, along with a rapid increase in the gas pressure (not shown). Subsequently, a potential "rollover" occurs at the negative electrode in response to the reduction in oxygen partial pressure by the recombination.

To demonstrate the model's fidelity over a wide range of operating conditions, Fig. 6a shows simulation results of various charge curves from $C/10$ to $10C$. As expected, the higher the charging rate, the higher the polarization. It is interesting to observe that increasing the rate results in faster charge with the same efficiency, provided that no mass loss occurs. Unfortunately, the pressure profiles in Fig. 6b demonstrate that too much increase in the rate may result in open valve and gas venting, thus induce water loss in the battery. The result suggests that the battery can withstand a charging rate up to $1C$. Beyond $1C$, such high charging rate could drastically increase water loss. LAB manufacturers usually specify a maximum current for the charge regime, as well as a maximum voltage to avoid possible gas venting and cell aging processes to

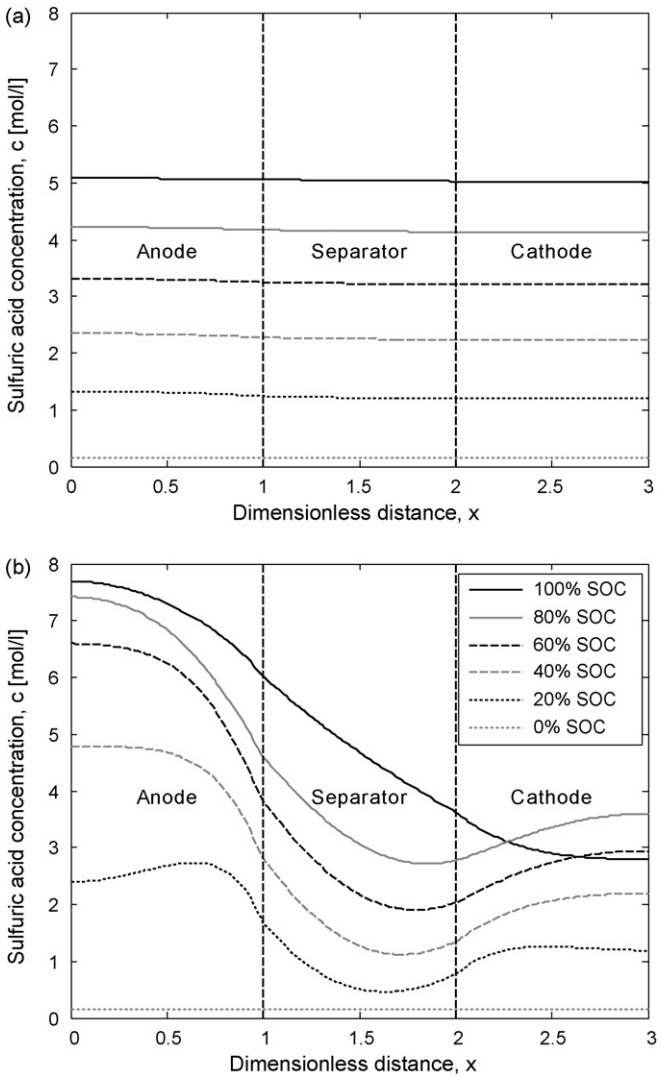

Fig. 7. Sulfuric acid concentration profiles simulated by steps of 20% SOC at (a) *C*/10 and (b) 10*C* in charge regime.

reduce water loss and grid corrosion that can harm battery service life. One should be cautioned that Fig. 6 has not been validated experimentally yet.

Additional utility that a mathematical model can offer is the ability of deriving mass-transport related properties inside the battery. For example, one can simulate acid concentration profiles at different charging rates to study transport limitation. Fig. 7a and b illustrates such profiles at *C*/10 and 10*C*, respectively. At *C*/10, acid diffusion is fast so that an acid concentration gradient is hardly observed. At 10*C*, a significant acid concentration gradient could be observed across a cell, illustrating the ionic transport limitation. Similar phenomenon has already been simulated at high discharge rates [17,18]. In the discharge regime, acid consumption and water liberation in the positive electrode lead to a dilution in acid concentration, which explains why a lower acid concentration is usually observed in the positive electrode than the negative electrode, as explained by Bode [21] (p. 78). In the charge regime, the opposite occurs; the acid liberated in the positive electrode, leading to a higher concentration than in the negative electrode. Experimentally, high rates generate high concentration gradients between the positive electrode and the rest of the cell, until the diffusion equalizes them after few minutes or hours, depending on the duration this rate has been applied.

To refine this model, some additional work is still needed to improve the model capability and fidelity. Simulation of the rest period preceding the charge regime and the impact from the rest on battery behavior are major issues that need to be addressed. Moreover, the gas composition and pressure shall be measured accurately to derive secondary reaction kinetics for model validation. Through such validation, the model should be able to predict the amount of water loss in the charge regime. A more careful analysis of the experimental charge curve indicates that the primary reactions are more complex than simple $PbSO_4$ transformation. Bernardi et al. [15] have recently shown that satisfactory simulation results can be obtained by a dissolution-transport mechanism in the negative electrode and a solid-state mechanism for the positive electrode. If such validation on charging curves was achieved at various rates, the model would be ready for dealing with more complex charging protocols in a common setting.

4. Conclusion

It is more complicated to simulate charge regimes than discharge in LAB modeling. The complexity comes from the secondary reactions involving gas evolution and recombination. The charge regime in the LAB also comprises multi-steps (typically comprising CC and CV), making the simulation challenging. The initial condition of the charge regime depends on the previous EOD conditions; thus, the LAB model has to be modified substantially to include an additional set of equations accommodating the above complexity.

In this work, we showed that a successful simulation of the LAB charge regime can be conducted with high fidelity. It is a prerequisite to acquire an accurate model that can consistently simulate discharge over a substantial range of conditions. With proper modifications, this model can then be applied successfully to the charge regime to yield accurate and high fidelity results. Simple galvanostatic charge at *C*/10 was illustrated with prior discharge regimes performed from *C*/10 to 10*C*. The high fidelity in the simulation gives an accurate account for the role played by each electrode reaction in polarization, nature of the polarization (from reaction kinetics and mass transport), and charging efficiency. We can extend the simulation beyond the range the model has been validated for. The results comply with experimental observations up to the maximum charging rate specified by most LAB manufacturers.

Acknowledgments

Supports from the Hawaii Center for Advanced Transportation Technologies (via the U.S. Air Force Advanced Power Technology Office at the Robins Air Force Base, GA) and Southwest Research Institute are appreciated.

References

[1] W.H. Tiedemann, J. Newman, Battery design and optimization: mathematical modeling of the lead-acid cell, in: The Electrochemical Society Softbound Proceedings Series, Princeton, NJ, 1979, p. 23.
[2] H. Gu, T.V. Nguyen, R.E. White, J. Electrochem. Soc. 134 (1987) 2953.
[3] T.V. Nguyen, R.E. White, J. Electrochem. Soc. 137 (1990) 2998.
[4] D.M. Bernardi, H. Gu, J. Electrochem. Soc. 140 (1993) 2250.
[5] T.V. Nguyen, R.E. White, Electrochim. Acta 38 (1993) 935.
[6] D.M. Bernardi, M.K. Carpenter, J. Electrochem. Soc. 142 (1995) 2631.
[7] J. Landfors, D. Simonsson, A. Sokirko, J. Power Sources 55 (1995) 217.
[8] W.B. Gu, C.Y. Wang, B.Y. Liaw, J. Electrochem. Soc. 144 (1997) 2053.
[9] E. Karden, P. Mauracher, F. Schöpe, J. Power Sources 64 (1997) 175.
[10] J. Newman, W. Tiedemann, J. Electrochem. Soc. 144 (1997) 3081.
[11] A. Tenno, R. Tenno, T. Suntio, J. Power Sources 103 (2001) 42.
[12] W.B. Gu, G.Q. Wang, C.Y. Wang, J. Power Sources 108 (2002) 174.
[13] A. Tenno, R. Tenno, T. Suntio, J. Power Sources 111 (2002) 65.
[14] V. Srinivasan, G.Q. Wang, C.Y. Wang, J. Electrochem. Soc. 150 (2003) A316.
[15] D.M. Bernardi, R.Y. Ying, P. Watson, J. Electrochem. Soc. 151 (2004) A85.
[16] V. Esfahanian, F. Torabi, A. Mosahebi, J. Power Sources 176 (2008) 373.

[17] M. Cugnet, S. Laruelle, S. Grugeon, B. Sahut, J. Sabatier, J.-M. Tarascon, A. Oustaloup, J. Electrochem. Soc. 156 (2009) A974.
[18] M. Cugnet, M. Dubarry, B.Y. Liaw, ECS Trans. 25 (2010) 223.
[19] C.P. Wales, A.C. Simon, J. Electrochem. Soc. 128 (1981) 236.
[20] C.P. Wales, A.C. Simon, J. Electrochem. Soc. 128 (1981) 2512.
[21] H. Bode, Lead-acid Batteries, John Wiley & Sons, New York, 1977.
[22] Y. Yamaguchi, M. Shiota, Y. Nakayama, N. Hirai, S. Hara, J. Power Sources 85 (2000) 22.
[23] D. Berndt, J. Power Sources 95 (2001) 2.
[24] B. Bensmann, R. Hanke-Rauschenbach, E. Meißner, I. Koch, K. Sundmacher, J. Electrochem. Soc. 157 (2010) A243.